Optics Communications 322 (2014) 1–7

Contents lists available at ScienceDirect

Optics Communications

journal homepage: www.elsevier.com/locate/optcom

Simulation of transmitted spectrum in metallic photonic crystals by boundary element method

Sima Mohammad Aminifard, Mahdi Sovizi *

Physics Department, Vali-e-Asr University of Rafsanjan, Rafsanjan, Kerman 7718897111, Iran

ARTICLE INFO

Article history:
Received 21 December 2013
Received in revised form
24 January 2014
Accepted 31 January 2014
Available online 15 February 2014

Keywords:
Metallic photonic crystals
Resonance wavelength
Boundary element method (BEM)

ABSTRACT

In this study, scattered and transmitted terahertz waves of a given structure consisted of metallic rods were simulated using the boundary element method (BEM). Through the proposed model, the transmission spectrum of metallic photonic crystals was calculated and it has been shown that the rotation of a structure with an anisotropic cavity leads to the shift of the resonance wavelength. In this work, a tunable multi-chromatic filter was designed whose resonance wavelengths were varied at incident angles of 0° and 90°. The effects of rod materials and the number of rods' rows on the position and quality factor of resonance peaks in finite metallic photonic crystals have also been investigated.

1. Introduction

Photonic crystal is an artificially fabricated structure whose structure period has the same order in magnitude as wavelength of the incident electromagnetic wave [1]. Their key feature is a frequency region in which the propagation of any electromagnetic radiation is prohibited [2]. According to the fact that the dielectric constant of metals is very different to that of else dielectric materials, it results in special properties of metallic photonic crystals, such as big gaps, losses, and the existence of "cutoff frequencies". For most of photonic crystals, first photonic pass band evolves from zero frequency to its edge at which first PBG starts then. However, in the cases of 2D metallic photonic crystals, the first PBG usually evolves from zero frequency to a frequency defined as "cutoff frequency" for TE (electric field parallel to the metallic cylinders) waves [3]. Also by introducing a defect into the structure real states within the stop band can occur [4] which produces a peak in the scattering cross section of the cluster due to the resonant tunneling through the defect mode. One thing that is important in photonic crystals with defect is quality factor of modes, which is a measure of how many oscillations take place in a cavity, originates from the fact that the amplitude of their wave functions decreases exponentially with the distance from the center of the defect structure. Furthermore, the more interesting application of resonant cavities is enhancing the efficiency of lasers, taking advantage of the fact that the density of states at the resonant frequency is very high [5].

In some references the multiple scattering theory is applied to a Drude type metallic system of cylinders without dissipation where the eigen frequencies of defect modes are calculated as a function of the defect size [6]. So the defect frequency inside a PBG can, in principle, be selected by designing the shape or the size of a local defect in photonic crystals [5]. To extend the versatility and application of PCs with defects, it is desirable to tune the defect modes. Several studies have concentrated on tuning the forbidden bands [7,8] light switching, and on tuning defect modes [9–12]. On the other hand photonic crystals operating at terahertz frequencies are particularly interesting, since investigating the transmission mechanisms of photonic crystals in the terahertz range allows easy fabrication of samples, as the wavelengths are comparably large (1 THz corresponds to 300 μm) [13]. Also metal constituents are particularly suitable for the construction of photonic crystals in the terahertz range, as the losses caused by the finite conductivity of the metal are small at these relatively low frequencies [14].

It has already used of different approaches such as plane wave method [15], transfer matrix method [5], and boundary element method [16] to calculate the position of photonic band gap.

For instance Nemec et al. have demonstrated a defect mode in a one dimensional PC that can be tuned in terahertz range [9] and Fan et al. have demonstrated that the position of PBG is remarkably shifted when the refractive index of LC is tuned by different external electric by FEM method [8]. Also Kaliteevski et al. have theoretically proposed a type of pass band filter which operate in the terahertz frequency regime by possessing two separate pass bands utilizing the distinction between positive and negative refraction in a photonic crystal prism [17], Moreover Xiao et al. have designed a tunable photonic crystal filter at visible band by FDTD method [11] and Sedghi et al. have considered 2D MPCs in

* Corresponding author. Tel.: +98 391 320 2428; fax: +98 391 320 2429.
E-mail address: msovizi@gmail.com (M. Sovizi).

http://dx.doi.org/10.1016/j.optcom.2014.01.086
0030-4018

square, triangular and honeycomb, with different geometry of rods and discussed the effect of shapes and orientation of scatters on the PBG by revised form of PWM (RPWM) [18].

Hassanzadeh et al., by considering real refractive index for rods, found the position of band gap of dielectric photonic crystals by using boundary element method [16].

The boundary element method has advantages over other numerical methods, including finite difference method (FDM) and finite element method (FEM), such as decreasing time and increasing precision of the calculation. Since in this method the integrations are only taken over the boundaries, it leads to a decreased computation time and increased computation speed and precision. On the other hand, in the boundary element method, the Green function is employed to obtain the field in the boundary whereas in other methods, the field is estimated into the boundary.

In this research, by the numerical method of BEM, the scattered field of a structure consisted of metallic rods has been simulated. After validation of the results and comparison with other related studies, the transmission spectrum is obtained for various structures and it is shown that by rotating a structure with an anisotropic cavity, the resonance wavelength changes. Hence, the effect of rod material on quality factor of resonance peaks is studied. Furthermore, a multi-chromatic filter with a triangular lattice is introduced that works in the range of terahertz frequency. The effect of changing the number of rod rows on the transmission spectrum and resonance peak characteristics have also been investigated.

2. Theory

It is assumed that an array of N metallic rods with a circular cross section of radius a_i and a complex refractive index of $\tilde{n}_i(\omega)=\sqrt{\tilde{\kappa}_i(\omega)}$ are placed in an infinite medium with the refractive index of $n_a=\sqrt{K_a}$. The $\tilde{\kappa}_i(\omega)$ and K_a are the complex dielectric constant of rods and dielectric constant of background medium, respectively. The rods are considered as with infinite length and parallel to z-axis (Fig. 1) which their position are denoted by (x_i, y_i). The index $i\in\{1,\ldots,N\}$ shows the ith rod. The monochromatic electromagnetic wave in TE or TM mode with the angular frequency ω and wave vector $\vec{k}$, placed in the xy-plane, radiates on rods through an arbitrary incident angle. The incident beam after reflection of rods' surface are partially scattered to different directions and partially penetrates into the rods in which the penetration depth depends on the skin depth. The incident field, scattered field, and internal fields of metallic rods are specified as $\phi_{inc}\hat{z}$, $\phi_s\hat{z}$ and $\phi_i\hat{z}$. The quantity ϕ in TE and TM mode represents E_z and H_z, respectively. The Helmholtz equation for the monochromatic wave in a non-magnetic conductor is written as below:

$$\nabla^2\phi_i+k_i^2\phi_i=0 \tag{1}$$

It should be noted that the magnitude of the wave vector is a complex quantity and is obtained as [19]:

$$k_i=\omega\tilde{n}_i(\omega)/c=\omega\sqrt{\tilde{\kappa}_i(\omega)}/c \tag{2}$$

The complex dielectric coefficient $\tilde{\kappa}_i(\omega)$ is calculated using Drude–Lorentz theory:

$$\tilde{\kappa}_i(\omega)=1-\frac{\omega_p^2}{\omega(\omega+i\omega_\tau)} \tag{3}$$

where ω, ω_p, and ω_τ are the incident beam frequency, plasma frequency, and damping frequency, respectively, and the numerical values of these parameters are found in references. For example, ν_p is equal to 2175 and 1914 THz, and ν_τ is equal to 6.5 and 8.34 THz for gold (Au) and copper (Cu), respectively [20].

By taking a conductivity of zero for the background medium, the electric and magnetic fields in both TE and TM modes hold in Helmholtz equation:

$$\nabla^2\phi_a+k_a^2\phi_a=0,\quad k_a=\omega n_a/c \tag{4}$$

where the real quantity k_a is the magnitude of the wave vector in background medium and $\phi_a=\phi_{inc}+\phi_s$ is the total field in this medium which is equal to the sum of the incident and scattered fields. Since the operator ∇^2 is a linear operator and the incident wave satisfies the Helmholtz equation, so the scattered wave should also satisfy in this equation:

$$\nabla^2\phi_s+k_a^2\phi_s=0 \tag{5}$$

Boundary conditions governing fields on the interface of rods and the medium are expressed as:

$$\phi_i=\phi_{inc}+\phi_s \tag{6}$$

$$\frac{\partial\phi_i}{\partial n}=\alpha\left(\frac{\partial\phi_{inc}}{\partial n}+\frac{\partial\phi_s}{\partial n}\right) \tag{7}$$

The coefficient α for TE and TM mode is equal to 1 and $\tilde{\kappa}_i(\omega)/K_a$, respectively. Regarding to boundary conditions of (6) and (7) and solving differential Eqs. (1) and (5), we can calculate scattered fields of metallic arrays. In this study, using boundary element method, these equations are solved. In this method through the second form of Green's theorem and Green functions, differential equations are converted to integral equations. Green's equations corresponding to differential Eqs. (1) and (5) are expressed by [21]:

$$\nabla^2G_{i,a}(\vec{X},\vec{X}')+k_{i,a}^2G_{i,a}(\vec{X},\vec{X}')=-\delta(\vec{X}-\vec{X}') \tag{8}$$

where G_i and G_a are Green functions corresponding to internal areas of the rods and the background medium, respectively. In 2D problems, these functions are [21]:

$$G_{i,a}(R)=iH_0^1(k_{i,a}R)/4 \tag{9}$$

where H_0^1 is the zero order of first kind of Hankel function and R is the separation from point $\vec{X}$ to $\vec{X}'$ obtain by:

$$R=|\vec{X}-\vec{X}'| \tag{10}$$

The second form of Green's theorem is [21]:

$$\int_\Omega\phi(\vec{X})\nabla^2\psi(\vec{X})-\psi(\vec{X})\nabla^2\phi(\vec{X})d\Omega=\oint_\Gamma\phi(\vec{X})\frac{\partial\psi(\vec{X})}{\partial n}-\psi(\vec{X})\frac{\partial\phi(\vec{X})}{\partial n}d\Gamma \tag{11}$$

In this relation, $\phi(\vec{X})$ and $\psi(\vec{X})$ are scalar functions in the area Ω surrounded by the boundary Γ. Considering $\psi(\vec{X})=G_{i,a}(\vec{X},\vec{X}')$

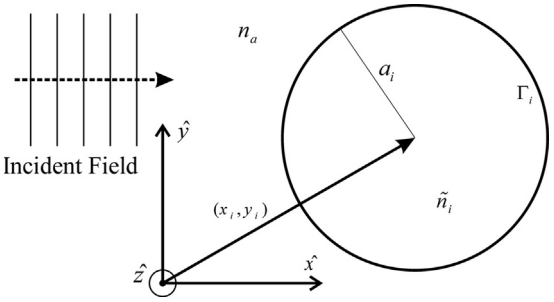

Fig. 1. A schematic of the incident wave and the cross section of one of rods; $\tilde{n}_i(\omega)$ is the refractive index of rod i and n_a is the refractive index of the background medium.

and $\phi(\vec{X}) = \phi_{i,s}(\vec{X})$, and using (11), Eqs. (1) and (5) are converted to:

$$C(\vec{X}')\phi_i(\vec{X}') = \oint_{\Gamma_i} G_i(\vec{X}, \vec{X}')\frac{\partial \phi_i(\vec{X})}{\partial n} - \phi_i(\vec{X})\frac{\partial G_i(\vec{X}, \vec{X}')}{\partial n} d\Gamma,\ i = 1, \ldots, N \tag{12}$$

$$C(\vec{X}')\phi_s(\vec{X}') = \oint_{\Gamma_a} G_a(\vec{X}, \vec{X}')\frac{\partial \phi_s(\vec{X})}{\partial n} - \phi_s(\vec{X})\frac{\partial G_a(\vec{X}, \vec{X}')}{\partial n} d\Gamma \tag{13}$$

For each area, $C(\vec{X}')$ is calculated as below [22]:

$$C(\vec{X}') = -\oint_{\Gamma} \frac{\partial G(\vec{X}, \vec{X}')}{\partial n} d\Gamma \tag{14}$$

The internal area of the ith rod, its surrounding boundary, background area, and the boundary surrounding the background are denoted by Ω_i, Γ_i, Ω_a and Γ_a, respectively. As shown in Fig. 2, it can be seen that Γ_a includes all Γ_i and Γ_∞ where, Γ_∞ is a geometric boundary that encompasses all the crystal in very far

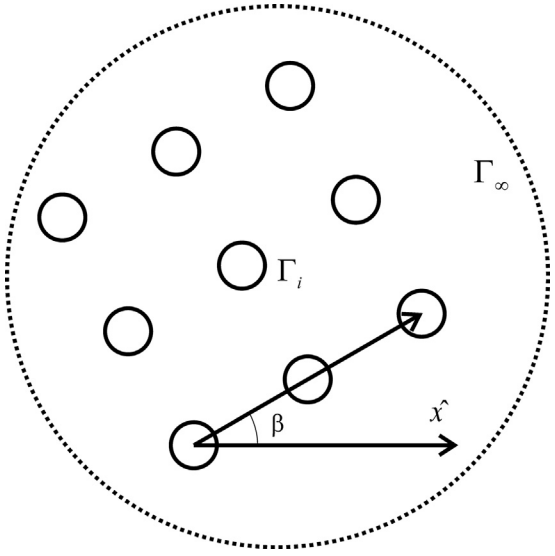

Fig. 2. The crystal cross section which is rotated by angle β around the z-axis. Γ_i is the boundary of rod i and Γ_a is the boundary surrounding the background medium, which is formed by a boundary encompassing the medium at infinite (Γ_∞) and all boundaries surrounding the rods (Γ_i).

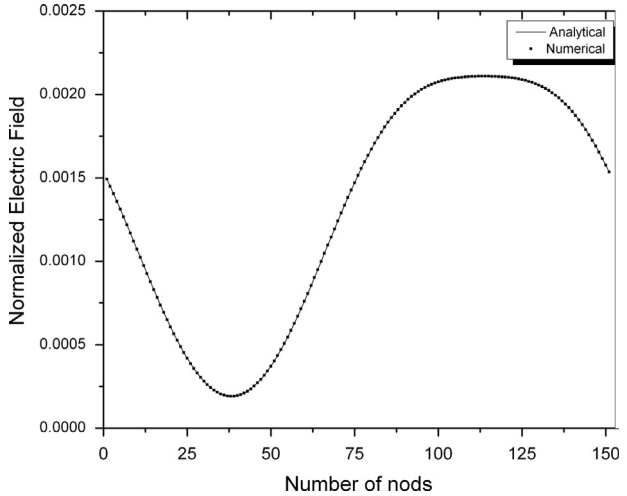

Fig. 3. The electric field in the rod's surface by numerical method of boundary element (dots) and analytical methods (solid line); the electric field is normalized relative to amplitude of the incident field.

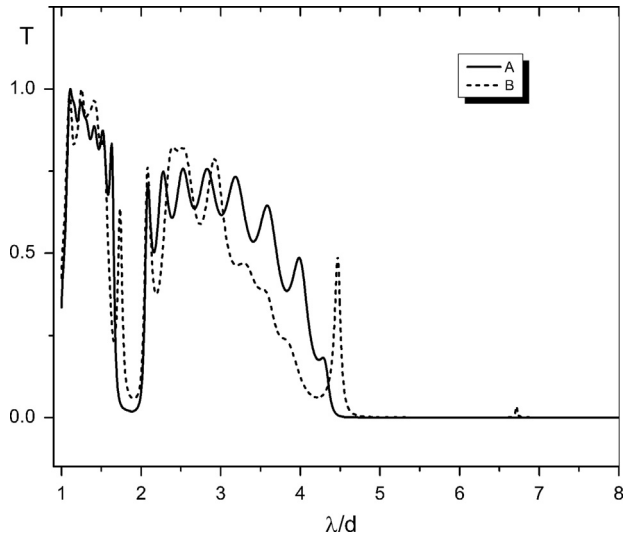

Fig. 4. The transmission spectrum of a metallic photonic crystal with 9×9 copper rods before (diagram A) and after removing 3×3 rods from its center (diagram B).

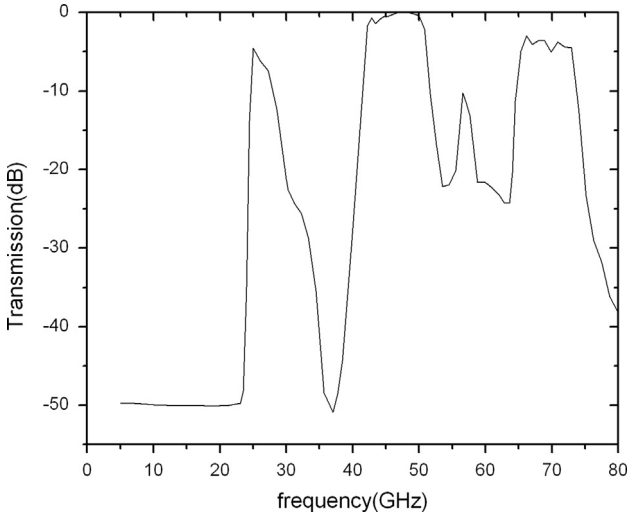

Fig. 5. The transmission spectrum of a square lattice with 7×14 copper rods by BEM.

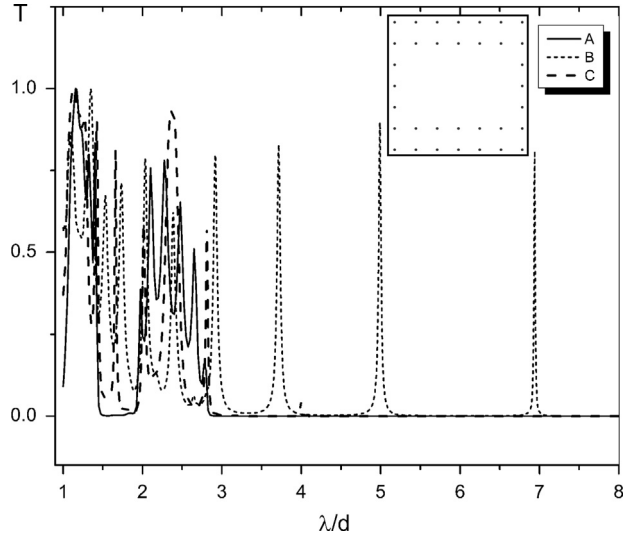

Fig. 6. The transmission spectrum of a square lattice with 7×7 rods before (diagram A) and after removing 3×5 rods at rotation angle of $\beta = 0^\circ$ (diagram B) and $\beta = 90^\circ$ (diagram C) and a representation of 7×7 crystal after removing 3×5 rods at $\beta = 0^\circ$.

distances. Therefore, Eq. (13) is changed to:

$$C(\vec{X}')\phi_s(\vec{X}') = \sum_{i=1}^{N} \oint_{\Gamma_i} -G_a(\vec{X},\vec{X}')\frac{\partial\phi_s(\vec{X})}{\partial n}+\phi_s(\vec{X})\frac{\partial G_a(\vec{X},\vec{X}')}{\partial n}d\Gamma + \oint_{\Gamma_\infty} G_a(\vec{X},\vec{X}')\frac{\partial\phi_s(\vec{X})}{\partial n}-\phi_s(\vec{X})\frac{\partial G_a(\vec{X},\vec{X}')}{\partial n}d\Gamma \quad (15)$$

It should be noted that if the point $\vec{X}$ is placed on the boundaries of Γ_i, there will be a relation as:

$$\left.\frac{\partial}{\partial n}\right|_{\Gamma_a} = -\left.\frac{\partial}{\partial n}\right|_{\Gamma_i} \quad (16)$$

Since the boundary of Γ_∞ has been assumed in distant separations from rods and the scattered field ϕ_s is damping as the separation from rods increases, so in Eq. (15) the integral over Γ_∞ in respect for other terms can be ignored. Hence:

$$C(\vec{X}')\phi_s(\vec{X}') = \sum_{i=1}^{N} \oint_{\Gamma_i} -G_a(\vec{X},\vec{X}')\frac{\partial\phi_s(\vec{X})}{\partial n}+\phi_s(\vec{X})\frac{\partial G_a(\vec{X},\vec{X}')}{\partial n}d\Gamma \quad (17)$$

Using boundary conditions of (6) and (7), Eq. (12) is rewritten as:

$$C(\vec{X}')\phi_i(\vec{X}') = \oint_{\Gamma_i}\alpha G_i(\vec{X},\vec{X}')\frac{\partial\phi_s(\vec{X})}{\partial n}-\phi_s(\vec{X})\frac{\partial G_i(\vec{X},\vec{X}')}{\partial n}d\Gamma + \oint_{\Gamma_i}\alpha G_i(\vec{X},\vec{X}')\frac{\partial\phi_{inc}(\vec{X})}{\partial n}-\phi_{inc}(\vec{X})\frac{\partial G_i(\vec{X},\vec{X}')}{\partial n}d\Gamma \quad (18)$$

Eqs. (17) and (18) are coupled integral equations. By taking these equations, it can be found that if the scattered wave and its normal derivative over the rod's boundary are determined, then we are able to obtain $\phi_i(\vec{X}')$ and $\phi_s(\vec{X}')$ at any arbitrary point $\vec{X}'$ inside or outside of the rods. Then by superposition of the incident field and the scattered field, the total filed at any given point in the outside area of the rods can be calculated. For this purpose, we have solved these equations through conventional boundary element methods and have found $\phi_s(\vec{X})$ and $\partial\phi_s(\vec{X})/\partial n$ on the boundaries of the rods. Since in this approach, only the boundary of rods is meshed, this procedure easily is done. In addition, high speed and precision are advantages of this method.

3. Results and discussions

In this study, it is assumed that the incident wave in TE polarization (the electric field of incident wave is parallel to the rod axis) which propagates along x-axis, irradiates on photonic crystals including metallic rods in the air, which is rotated by angle of β around the z-axis (see Fig. 2).

Table 2
Resonance peak characteristics of a square lattice with 7×7 copper and gold rods with a 5×3 cavity.

	λ/d	$\delta\lambda/d$	Q factor
Cu	3.99	8.51×10^{-3}	468.86
	2.97	1.55×10^{-1}	19.16
Au	3.99	8.02×10^{-3}	497.50
	2.97	2.86×10^{-2}	103.84

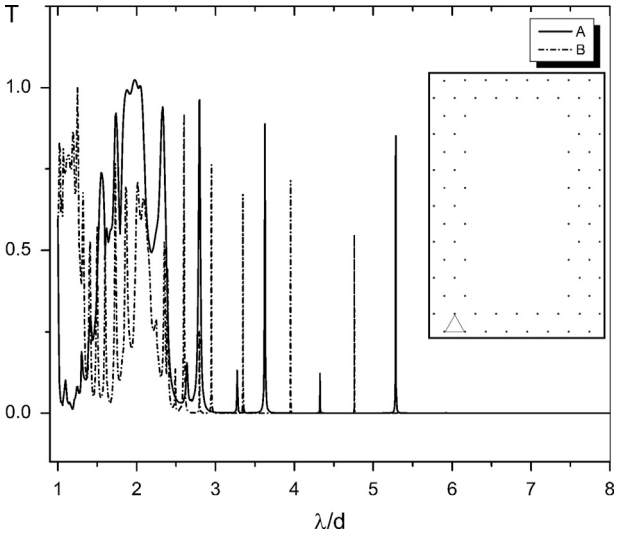

Fig. 7. The transmission spectrum of a triangular lattice with 17×15 rods after removing 9×11 rods at rotation angle of $\beta=0^\circ$ (diagram A) and $\beta=90^\circ$ (diagram B) and a representation of crystal structure with 17×15 rods after removing 9×11 rods at rotation angle of $\beta=0^\circ$.

Table 1
Resonance peak characteristics of a square lattice with 7×7 rods after removing 3×5 rods.

Number of modes	$\beta=0^\circ$	$\beta=40^\circ$	$\beta=45^\circ$	$\beta=50^\circ$	$\beta=90^\circ$
First mode					
λ/d	2.92	2.98	2.98	2.98	2.97
$\delta\lambda/d$	5.56×10^{-2}	3.88×10^{-2}	4.00×10^{-2}	4.62×10^{-2}	1.55×10^{-1}
Q factor	52.51	76.80	74.50	64.50	19.16
Second mode					
λ/d	3.72	3.72	–	–	–
$\delta\lambda/d$	4.85×10^{-2}	5.04×10^{-2}	–	–	–
Q factor	76.70	73.80	–	–	–
Third mode					
λ/d	–	3.99	3.99	3.99	3.99
$\delta\lambda/d$	–	9.37×10^{-3}	9.34×10^{-3}	8.84×10^{-3}	8.51×10^{-3}
Q factor	–	425.82	427.19	451.35	468.86
Fourth mode					
λ/d	4.99	5.00	4.99	5.01	–
$\delta\lambda/d$	3.56×10^{-2}	3.61×10^{-2}	5.69×10^{-2}	2.58×10^{-1}	–
Q factor	140.16	138.50	87.69	19.41	–
Fifth mode					
λ/d	6.94	6.94	6.94	6.94	–
$\delta\lambda/d$	1.65×10^{-2}	1.66×10^{-2}	1.67×10^{-2}	2.52×10^{-2}	–
Q factor	420.60	418.07	415.56	275.39	–

In order to verification of the proposed model, it is assumed that the incident beam with wavelength of 1 mm radiates on one or more (two or three) copper rods with a radius of 0.05 mm. The diffraction pattern of the field is obtained by analytical and numerical methods. The average absolute value of relative error was calculated as less than 0.1% for numerical results versus analytical results, for choosing 151 nodes on the boundary of each rod (see Fig. 3). In Fig. 3, the vertical axis represents the calculated electric field $\phi_a$on the boundary nodes of the rod.

Because an analytical solution for complex structures is impossible, then for more investigating the validation of the proposed model, obtained results have been compared with available results in Ref. [23]. For this purpose, the position of photonic band gap for a structure consisted of 9×9 copper rods with circular cross section (with a radius of $a_i=0.01$ mm) for a square lattice with lattice constant of $d=1$ mm has been calculated before and after removing 3×3 rods from the structure center (see Fig. 4). It is observed that the transmission spectrum of the perfect structure for wavelengths of $\lambda/d>4.5$ can be ignored (diagram A), but after removing 3×3 rods, the resonance peaks have been produced in the frequency band gap (diagram B). The produced cavity in the crystal acts as a resonator and the incident wave on the crystal resonates in two certain wavelengths in this cavity. Using the proposed model in this work, the resonance wavelengths of $\lambda_1/d=4.47$ and $\lambda_2/d=6.71$ are achieved. These wavelengths are reported by Guida et al. by considering the mean field approximation and definition of relative permittivity as $\lambda_1/d=4.45$ and $\lambda_2/d=6.7$ [23].

To further verify the correctness of the model, we have calculated the transmission spectrum for a structure composed of 7×14 copper rods (with a radius of $a_i=1$ mm), arranged in a square lattice structure for a lattice constant of 6 mm (Fig. 5). Also the transmission spectrum of the structure has been calculated using FDTD method [24]. As can be seen, the transmission spectrums obtained by the BEM and FDTD methods are in good agreement with each other.

Afterwards, the effects of anisotropy of the cavity on resonance wavelengths are investigated. For this purpose, a rectangular cavity is formed inside a crystal of a square lattice with lattice constant of $d=1$ mm consist of 7×7 copper rods with a radius of $a_i=0.08$ mm. The transmission spectrum is presented at rotation angles of $\beta=0^\circ$ and $\beta=90^\circ$ in Fig. 6. In diagram A, the transmission spectrum of the perfect crystal before removing rods is

Table 3
Resonance peak characteristics of a triangular lattice with 17×15 rods after removing 9×11 rods.

$\beta=0^\circ$				$\beta=90^\circ$			
Number of modes	λ/d	$\delta\lambda/d$	Q factor	Number of modes	λ/d	$\delta\lambda/d$	Q factor
1	2.64547	0.00951	278.17	1	2.60112	0.00878	296.25
2	2.80494	0.00982	285.63	2	2.79648	0.00240	1165.20
3	3.27534	0.00141	2322.93	3	2.94776	0.00298	989.18
4	3.62578	0.00145	2500.53	4	3.34756	0.00166	2016.60
5	4.32375	0.00044	9826.70	5	3.95119	0.00087	4541.59
6	5.28258	0.00044	12005.86	6	4.76020	0.00056	8500.35

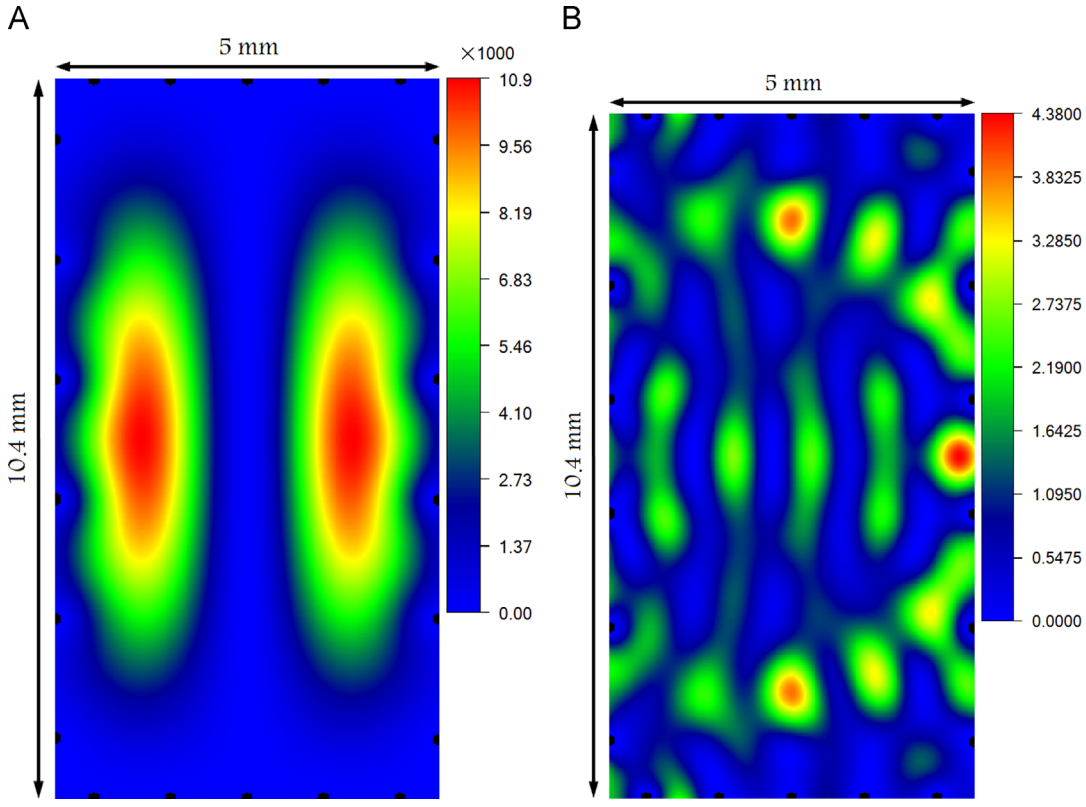

Fig. 8. The normalized intensity calculated at resonant (A) and non-resonant (B) wavelengths of $\lambda/d=5.28258$ (corresponding to the wavelength at peak 6 of Table 3) and $\lambda/d=2$, respectively.

shown. Also diagram B and C shows the transmission spectrum of the crystal after removing rods at rotation angle of $\beta=0^\circ$ and $\beta=90^\circ$, respectively. The characteristics associated to resonance peaks including the ratio of resonance wavelength to lattice constant, the ratio of full width at half maximum (FWHM) to lattice constant, and the quality factor of resonance peaks at different angles are shown in Table 1. To find FWHM and quality factor of transmitted peaks, at first each peak was fitted to a Lorentz peak [3], then using the term $Q=\lambda/\delta\lambda$, quality factor has been calculated [25]. As seen in Table 1, by rotating the crystal from 40° to 50°, it is obvious that the quality factor of modes 2, 4 and 5 has been decreased and by a rotation of 90°, these modes have been disappeared. The rotation of the crystal resulted in producing the mode 3 so that the quality factor of this mode was maximized at the angle of 90°. The cause of resonance wavelength shift at different angles is that the effective length of the resonator along the incident wave varies at various angles and therefore the wavelength of defect mode will change.

In order to study the effect of rod material on the quality factors of resonance peaks, the transmission spectrum of a square lattice (lattice constant of $d=1$ mm) consisted of 7×7 rods (with a radius of $a_i=0.08$ mm) of which 5×3 rods are removed from the structure center, has been calculated. In Table 2, the resonance wavelength, full width at half maximum and quality factor are shown for this structure with gold and copper rods. As shown in Table 2, the quality factor of resonant modes in a crystal with gold rods is greater than copper rods. This increase is due to decreasing FWHM. Thus in order to achieve a structure with resonant modes having more quality factor, it can be used of a structure of gold rods.

The effect of anisotropy in the structure on properties of resonance peaks in a triangular lattice is also investigated. This structure includes 17×15 gold rods with a radius of $a_i=0.08$ mm and lattice constant of $d=1$ mm from which 9×11 rods are removed (see Fig. 7). The transmission spectrum of this structure at rotation angles of 0° (diagram A) and 90° (diagram B) is shown in Fig. 7. These structures can be used as polychromatic filters in Terahertz ranges and by rotating them to 90°, the transmitted peaks can be removed and the new peaks can be transmitted. In Table 3, the characteristics of resonance peaks are presented for a structure of 17×15 rods at $\beta=0^\circ$ and $\beta=90^\circ$.

For more understanding, we have investigated the intensity distributions at resonant and non-resonant wavelengths. As an example, corresponding to the case of Fig. 7 (diagram A), the normalized intensity calculated at $\lambda/d=5.28258$ and $\lambda/d=2$ is shown in Fig. 8A and B, respectively. It can be seen in Fig. 8A that field inside the cavity is intensive. It is typical intensity patterns when resonances in cavities take place. As a contrast, intensity pattern shown in Fig. 8B (corresponding to a wavelength in first pass band) is obviously different.

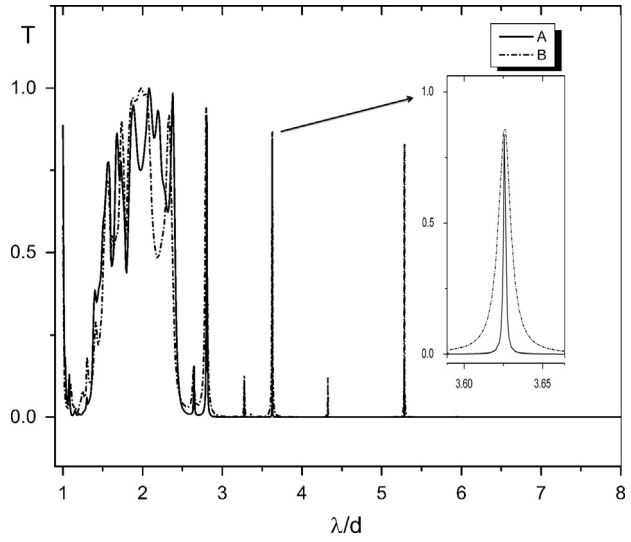

Fig. 9. The transmission spectrum of triangular lattice with 17×15 rods (diagram A) and 15×15 rods (diagram B) after removing 9×11 rods at rotation angle of $\beta=0^\circ$.

Table 4
Resonance peak characteristics of a structure with a triangular lattice with 15×15 gold rods after removing 9×11 rods.

$\beta=0^\circ$			
Number of modes	λ/d	$\delta\lambda/d$	Q factor
1	2.63777	0.02570	102.63
2	2.79674	0.02632	106.25
3	3.27524	0.00800	409.40
4	3.62574	0.00915	396.25
5	4.32443	0.00269	1607.59
6	5.28371	0.00402	1314.35

Then without changing the cavity, we changed the crystal 17×15 to a crystal with 15×15 rods by removing two lateral rows. The transmitted spectrum of crystals with 17×15 (diagram A) and 15×15 (diagram B) at $\beta=0^\circ$ is shown in Fig. 9. The characteristics of resonance peaks for the structure of 15×15 are presented in Table 4. As shown in Table 4, by removing the number of rows from laterals of the crystal, resonance wavelengths are almost unchanged, but FWHM changes which lead to a change in quality factors of peaks. As an example, the peak #4 in Fig. 9 is shown more clearly in the box.

4. Conclusion

In this research, using boundary element method, the scattered field from a given structure consisted of metallic rods has been simulated. After the validation of proposed model and comparison of our results with data reported by other researchers, the transmission spectrum of various crystal structures was calculated. By rotating a structure with anisotropic cavity, a polychromatic filter was introduced and it was found that by rotating the crystal and changing the effective length of the cavity, the resonance wavelength modes varied. In addition to crystals with square lattice, the effect of rotation in crystals with triangular lattice was also investigated and a tunable polychromatic filter was introduced which had wavelengths in millimeter ranges. This study due to its application of these filters at long wavelengths is important. Also the effect of changing the number of rods on the transmission spectrum and characteristics of resonance peaks were studied. It was found that as the number of rod rows is varied, the wavelength of resonant mode is unchanged and only the quality factor of modes is changed.

References

[1] K.s. Tang, Y.j. Xiang, S.c. Wen, Optoelectron. Lett 2 (2006) 118.
[2] J.D. Joannopoulos, S.G. Johnson, J.N. Winn, R.D. Meade, Photonic Crystals: Molding the Flow of Light, Princeton University Press, New Jersey, 2011.
[3] J. Yu, L.M. Li, C. Meng, Phys. B: Condens. Matter 407 (2012) 4738.
[4] R.D. Meade, K.D. Brommer, A.M. Rappe, J. Joannopoulos, Phys. Rev. B: Condens. Matter 44 (1991) 10961.
[5] R. Moussa, L. Salomon, F. De Fornel, H. Aourag, Phys. B: Condens. Matter 338 (2003) 97.
[6] T. Ochiai, J. Sánchez Dehesa, Phys. Rev. B: Condens. Matter 65 (2002) 245111.
[7] H. van Driel, S. Leonard, J. Schilling, R. Wehrspohn, in: Tuning of 2-D Silicon Photonic Crystals, Materials Research Society Symposium Proceedings, Cambridge University Press (2002) 383–390.
[8] F. Fan, S. Chang, Y. Hou, Sci. China Inf. Sci 55 (2012) 72.

[9] H. Nemec, P. Kuzel, L. Duvillaret, A. Pashkin, M. Dressel, M. Sebastian, Opt. Lett 30 (2005) 549.
[10] R. Pechstedt, P.S.J. Russell, T. Birks, Photonic Band Gap Materials, Springer, Southampton (1996) 445–452.
[11] H. Xiao, D. Yao, Phys. E (Low. Dimens. Syst. Nanostruct.) 27 (2005) 1.
[12] R. Ozaki, Y. Matsuhisa, M. Ozaki, K. Yoshino, Appl. Phys. Lett. 84 (2004) 1844.
[13] B. Reinhard, G. Torosyan, R. Beigang, Appl. Phys. Lett. 92 (2008) 201107.
[14] M. Sigalas, C. Chan, K. Ho, C. Soukoulis, Phys. Rev. B: Condens. Matter 52 (1995) 11744.
[15] K. Busch, S. John, Phys. Rev. E: Stat. Nonlinear Soft Matter Phys. 58 (1998) 3896.
[16] M. Hassanzadeh, M. Sovizi, M. Mohsseni, Opt. Int. J. Light Electron. Opt 124 (2013) 6869.
[17] M. Kaliteevski, S. Brand, J. Garvie Cook, R. Abram, J. Chamberlain, Opt. Express 16 (2008) 7330.
[18] A. Sedghi, M. Kalafi, A. Soltani Vala, B. Rezaei, Opt. Commun. 283 (2010) 2356.
[19] B.E. Saleh, M.C. Teich, B.E. Saleh, Fundamentals of Photonics, Wiley, New York, 1991.
[20] I. El Kady, M. Sigalas, R. Biswas, K. Ho, C. Soukoulis, Phys. Rev. B: Condens. Matter 62 (2000) 15299.
[21] J.D. Jackson, Classical Electrodynamics, University of California, Berkeley, 1998.
[22] F. París, J. Cañas, Boundary Element Method: Fundamentals and Applications, Oxford University Press, New York, 1997.
[23] G. Guida, D. Maystre, G. Tayeb, P. Vincent, J. Opt. Soc. Am. B: Opt. Phys. 15 (1998) 2308.
[24] F. Gadot, A. De Lustrac, J.M. Lourtioz, T. Brillat, A. Ammouche, E. Akmansoy, J. Appl. Phys. 85 (1999) 8499.
[25] J.H.E.P.W. Milonni, Physics Laser, John Wiley & Sons, Inc., Hoboken, New Jersey, 2010.